

## Synthesis and Characterization of $\text{La}_{0.9}\text{Sr}_{0.1}\text{Ga}_{0.8}\text{Mg}_{0.2}\text{O}_{3.6}$ Electrolyte for Intermediate Temperature Solid Oxide Fuel Cells (ITSOFC)

M. Kumar, A. Samson Nesaraj, I. Arul Raj and R. Pattabiraman

Central Electrochemical Research Institute, Karaikudi - 630 006

**Abstract** Experimental investigations on new materials for application as electrolyte in electrolyte supported planar Intermediate Temperature Solid Oxide Fuel Cells (ITSOFC) operating below 800 °C is in progress at our laboratory. Sr and Mg doped Lanthanum gallate (LSGM) powder was prepared by glycine - nitrate combustion method. The prepared LSGM powder is relatively finer than that prepared through other techniques such as solid-state reaction. The measurements comprising XRD, particle size, density, TGA/DTA were made. Thin sections of circular pellets were fabricated and annealed at different temperatures ranging between 1000 and 1300 °C. The sintering behaviour of LSGM was investigated to obtain information on the densification factor, relative percentage shrinkage/expansion in volume, while annealing and the resulting apparent porosity values. Bismuth oxide is found to be an effective sintering aid in general. So the effect of bismuth oxide addition on LSGM was investigated through sintering studies, XRD, TGA/DTA, SEM and conductivity measurements. The results obtained on LSGM with and without bismuth oxide addition are discussed with respect to the requirement of an electrolyte for ITSOFC applications.

### 1. Introduction

Lanthanum gallate,  $\text{LaGaO}_3$ , doped with Sr and Mg ( $\text{La,Sr}(\text{Ga,Mg})\text{O}_{3.8}$  (LSGM) is the promising electrolyte material for intermediate temperature solid oxide fuel cells (ITSOFCs) due to its high ionic conductivity. In recent years, after the discovery of the family of  $\text{LaGaO}_3$  - based electrolytes [1-6], a large amount of attention has been dedicated to the study of alternative electrolyte and mixed conducting materials with perovskite type structure [7]. The major features of the family of these materials are now well known. However, most of the work has been centered on the study of the structural characteristics, total ionic conduction and average ionic transport numbers within the conditions of practical relevance for fuel cell development. This is certainly an important approach for a first screening of the potential alternative electrolytes. But detailed information on the role of composition on electronic transport properties is still missing and deserves significant attention to improve the existing knowledge of the properties of these materials. The single-phase LSGM ceramic proved to be

difficult to synthesis. Some papers dealing with the synthesis of this electrolyte report the presence of traces of second phases [8]. In this study, we synthesized the LSGM electrolyte in the form of fine powder by glycine-nitrate combustion method. The physical and thermal properties of the synthesized powder are systematically evaluated. When circular components of these materials are annealed at different temperature, the degree of match in their thermal properties such as densification factor and shrinkage factor at above temperature range are measured and the conductivity measurement is carried out for LSGM, which are sintered at 1300 °C for 2 h. And we also aim to improve the conductivity values on LSGM (sintered at 1300 °C) with addition of bismuth oxide as sintering aid. The results obtained are discussed in order to qualify them for ITSOFC.

### 2. Experimental Description

*2.1. Powder Preparation.* High purity lanthanum nitrate, strontium nitrate, gallium nitrate and magnesium nitrate and glycine were used as starting materials. The stoichiometric

compositions of mixtures for the combustion were calculated using the total oxidising (O) and reducing (F) valencies of the components, which serve as a numerical coefficient for the stoichiometric balance, so that the oxidant to the fuel ratio is 1:1 for the LSGM synthesis. The LSGM was obtained by glycine-nitrate synthesis route, which involved rapid heating of an aqueous concentrated solution containing respective starting materials at 550 °C. The solution initially boiled, underwent rapid degradation and foaming followed by decomposition, generating gases such as CO<sub>2</sub>, N<sub>2</sub>, H<sub>2</sub>O. The gases ignited and burnt with temperature above 1000 °C, yielding voluminous oxide. The obtained oxide was calcined at 800 °C for 3 h to remove the unburnt materials and to obtain the most stable mixed oxide phases.

### 3. Sample Preparation and Characterization

**3.1. Physico-Chemical Characterization.** The combustion derived LSGM powders were characterized by XRD, density, particle size, and TGA/DTA. The XRD patterns were obtained with JEOL-8030 X-Ray Diffractometer using Cu-K $\alpha$  radiation. The density of the calcined LSGM powders was measured using pycnometer with xylene as the liquid medium. Horiba Laser Particle Size Analyser (LA-910) was used to determine the particle size distribution. The thermal characterization was carried out using PL Thermal Sciences unit at a heating rate of 10 °C/min in air.

The combustion-derived powders were made into circular test pellets under 5-ton uniaxial load. These pellets were sintered at different levels. The sintering behaviour and the porosity of those pellets were calculated for optimisation.

The combustion-derived LSGM powder and powder LSGM with various weight percent of bismuth oxide addition were mixed and crushed in an agate mortar and pelletized by applying 5-ton load. The LSGM pellets were subjected to sintering at various temperatures ranging from 1000 °C to 1300 °C and the LSGM pellets containing 0%, 1.2%, 2.4%, 3.6% and 4.8% bismuth oxide were subjected to sintering at constant temperature, 1300 °C for studying the effect of bismuth oxide addition at 1300 °C, 2 h dwell time. From the data obtained the sintering behaviour of LSGM powder was investigated. The conductivity measurements on LSGM with and without bismuth oxide pellets were carried out in air using ac impedance spectroscopy in the frequency ranging from 100 Hz to 100 kHz. The microstructures analysis of these pellets was studied by Scanning Electron Microscopy (SEM).

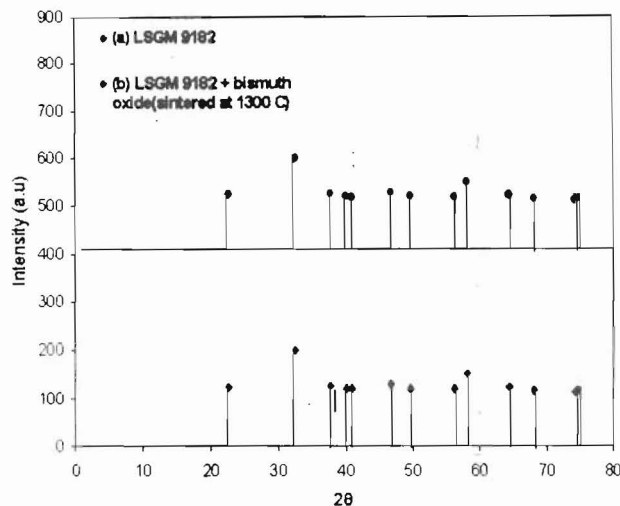


Fig. 1. XRD pattern of a) LSGM (sintered at 1300 °C) and b) LSGM with 4.8% bismuth oxide (sintered at 1300 °C).

### 4. Results and Discussions

**4.1. X-Ray Diffraction.** Figure 1a shows the XRD pattern obtained for LSGM (9182) perovskite oxide, which is indexed to the orthorhombic cell symmetry. The XRD data obtained on LSGM is given in Table 1. Goodenough and Feng [9] have reported that the LSGM (9182) phase was cubic, whilst Ishihara et al. [1] have reported an orthorhombic structure for this material. However, in this work, it is observed that the powder calcined at 1300 °C, 2 h also contained 5 wt.% of mixture of the undesired phases LaSrGaO<sub>4</sub> and LaSrGa<sub>3</sub>O<sub>7</sub>, as described in the literature [10]. Figure 1b clearly shows that the disappearance of bismuth oxide peaks in LSGM [11].

By using Scherrer equation, mean particle size

Table 1. Crystallographic properties obtained on LSGM 9182.

Properties	XRD data for LSGM9182
Crystal structure	Orthorhombic
Lattice parameter (Å)	A= 5.3741 B= 5.5433 C= 7.9145
Unit cell volume (Å) <sup>3</sup>	235.775
Theoretical density (g/cc)	6.7607
Crystallite size (nm)	10.773
Bulk density (g/cc)	0.044
Tap density (g/cc)	0.100
Absolute density (g/cc)	3.468

(crystallite size) of LSGM 9182 was calculated from the broadening of a specific diffraction peak. The equation used is:

$$D = \frac{0.9\lambda}{\beta \cos\theta}$$

where D is the average size of the crystallites, 0.9 is the Scherrer constant,  $\lambda$  is wave length of radiation,  $\beta$  is the peak width at half-height and  $\theta$  corresponds to the peak position. The crystallite size of LSGM 9182 was found to be 10.773 nm. It reveals that the densification of the LSGM 9182 compound at high temperature is less. Because of smaller crystallite size, the material has larger surface free energy [12]. Generally, the reduction of surface free energy is the driving force for sintering of the material [13] which is the reason for the low densification of LSGM 9182 at high temperature. Hence, in order to sinter the LSGM materials well even at low temperature, it was felt necessary to add bismuth oxide with various weight percent as sintering aid.

**4.2. TGA / DTA Studies.** The TGA/DTA pattern obtained on LSGM containing 4.8% bismuth oxide is shown in Fig. 2. From the Fig. 2, the disappearance of bismuth oxide peak in XRD was also verified from the results of the DTA of the sample, which doesn't show appearance of any sharp endothermic peak due to melting of bismuth oxide like observed in the case of LSGM using bismuth oxide as a sintering aid [11].

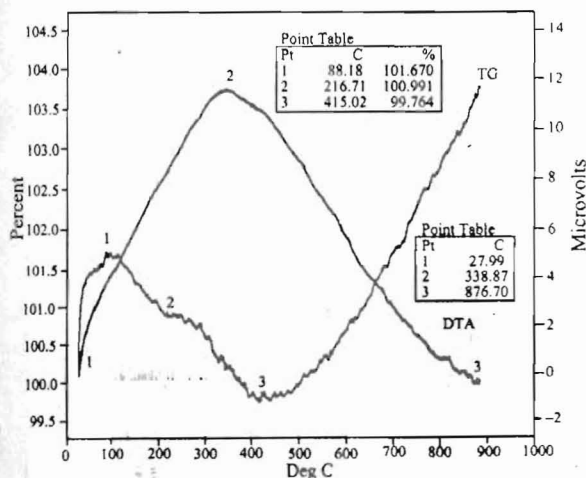


Fig. 2. TGA/DTA pattern of LSGM powder with 4.8% bismuth oxide.

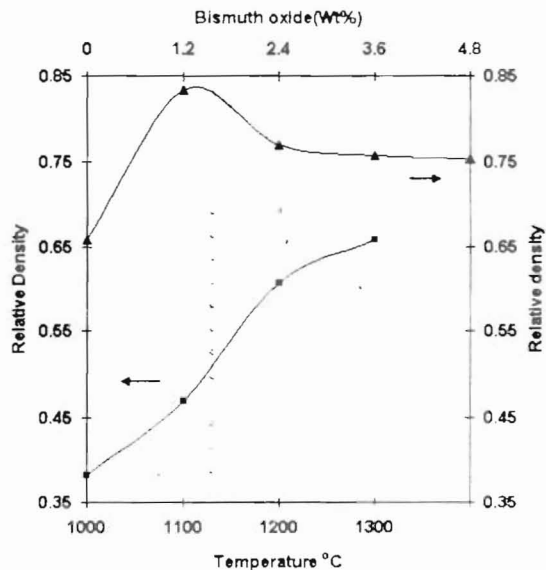


Fig. 3. The effect of temperature on relative density of the LSGM.

**4.3. Particulate Properties**

**4.3.1. Density Measurement.** The bulk, tap and absolute density values (measured using a pycnometer with xylene liquid) of LSGM powder was obtained and is given in Table 1. From the density data, it is drawn that the synthesized powders are fluffy and fine in nature.

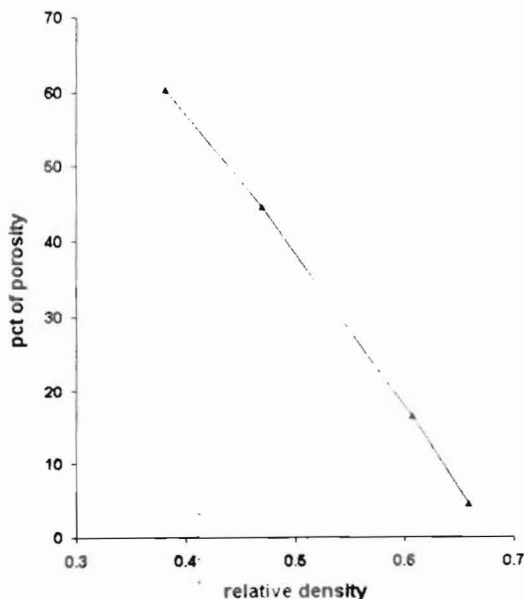


Fig. 4. The effect of relative density on percentage of porosity factor.

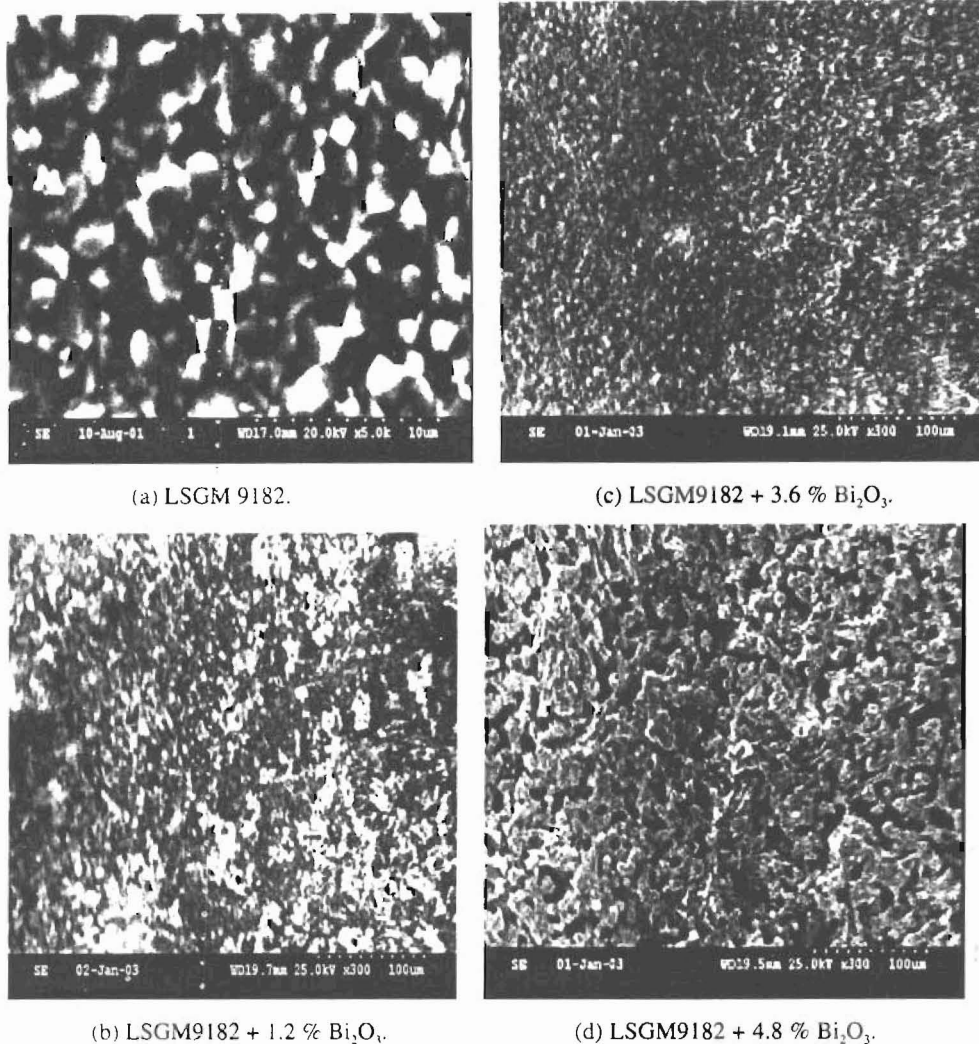


Fig. 5. SEM images of LSGM with and without bismuth oxide addition.

**4.3.2. Sintering Behaviour.** The sintering behaviour for LSGM was investigated in detail as a function of the sintering temperature. The relative density values were calculated from the sintering data and the apparent porosity values were estimated.

The effect of temperature and weight percent of bismuth oxide on relative density of the LSGM is shown in Fig. 3. The relative density increased with increasing temperature, and the relative density initially increased, then it slightly diminished and followed by constant with increasing bismuth oxide addition.

**4.3.3. Relative Density versus the Apparent Porosity.** The effect of relative density on the apparent porosity values of the sintered pellets made from the perovskite based LSGM materials is shown in Fig. 4. The percentage porosity value decreases with increasing relative density.

**4.3.4. Scanning Electron Microscope.** The effectiveness of bismuth oxide addition as sintering aid is also evident from the SEM fractograph of the sintered specimens as shown in Figs. 5a-d. A progressive change in microstructure with bismuth oxide is clearly visible. Figure 5a shows no grains with pores in the structure but small grains and small pores are formed with addition of bismuth oxide. Even 4.8 wt.% bismuth oxide addition is not sufficient enough for complete densification of LSGM 9182.

**4.3.5. Conductivity Measurement.** The ionic conductivity of LSGM 9182 with and without Bismuth oxide addition was measured by a two-probe complex impedance analysis. The conductivity value of LSGM with zero addition of bismuth oxide is  $10^{-2}$  S/cm at 800 °C, in which the LSGM component was sintered at 1300 °C for 2 h, but it was reported at >1500, for > 10 h in the literature [7,14,15,16

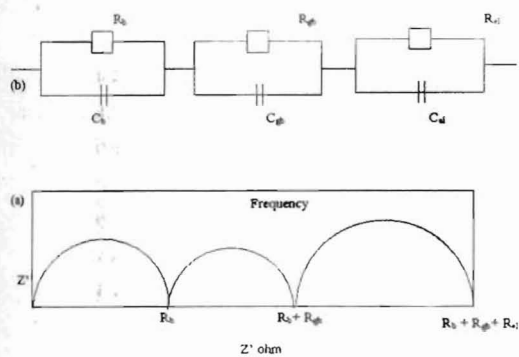


Fig. 6. An idealized equivalent circuit (b) and its corresponding impedance plot (a).  $C_b$ ,  $R_b$  and  $C_{gb}$ ,  $R_{gb}$  and  $C_{el}$ ,  $R_{el}$  represents resistance and capacitance for bulk, grain boundary and electrode process, respectively.

17]. The bismuth oxide addition was aimed to add as for increasing the sinterability and for increasing the oxide ion conductivity in LSGM.

The ionic conductivity( $\sigma$ ) has been measured in the range of temperature 500 °C to 800 °C. For all the samples of LSGM 9182 and mixed with 1.2% to 4.8% bismuth oxide all of which were sintered at 1200 °C for 2 h. In general, the a.c. impedance of an ionic conductor measured by a two probe method contains contributions from the bulk, grain boundaries and electrode/electrolyte interface, which can be reflected in a complex plane by three successive arc, as shown in Fig. 6a. The frequency increases from the right to the left across the plot. The arc at the high frequency end of the spectrum represents the bulk resis-

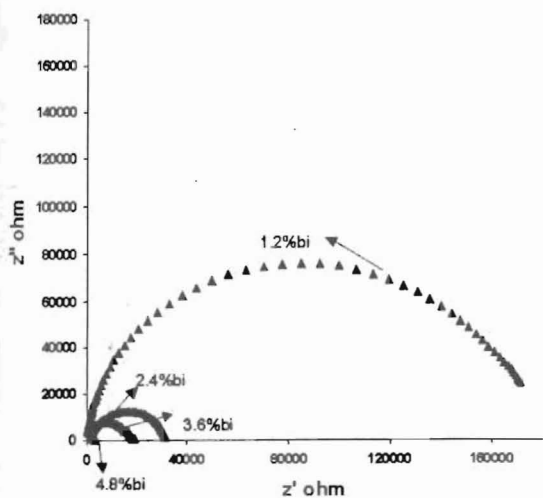


Fig. 7. Impedance plots of samples with different bismuth contents measured at 600 °C in air.

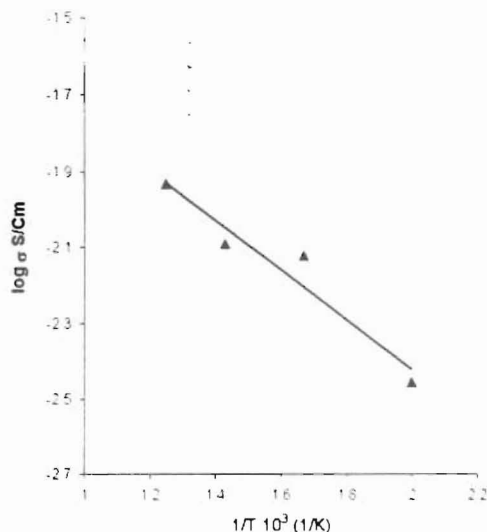


Fig. 8. Arrhenius plot for bulk conductivity of yttrium zirconate without bismuth oxide.

tivity; the arc at the middle of the spectrum is a consequence of the grain boundary effect; the low frequency arc is assigned to the electrode response. An idealized equivalent circuit for ceramic oxides corresponding to the impedance plot is shown in Fig. 6b. In a practical case, however, not all these arcs can be observed, depending on the nature of the samples and testing conditions. Figure 7 shows the impedance plots of samples with different bismuth contents measured at 500 °C in air. This figure clearly shows that the addition of bismuth oxide has a detrimental effect on grain boundary behaviour.

Figure 8 represents the plot of  $\log \sigma$  and  $1/T$  for the sample without bismuth oxide. A straight line was found and the conductivity increases with increasing temperature. The activation energy of the plot is 12.474 kJ.

The effect of bismuth oxide concentration on ionic conductivity for the samples with different temperatures is shown in Fig. 9. It found that straight lines are obtained for the samples with different temperatures. The energy of activation obtained for 500, 600 and 800 °C are -112.9, -239.3 and -122.54 J, respectively. As a result, higher energy of activation seems to be responsible for the higher conductivity in yttrium zirconate without bismuth.

From the results, it can be seen that the densification is increased by the addition of bismuth oxide, but the conductivity value obtained is lowered. The reason for lower conductivity is shown by scanning electron microscope analysis.

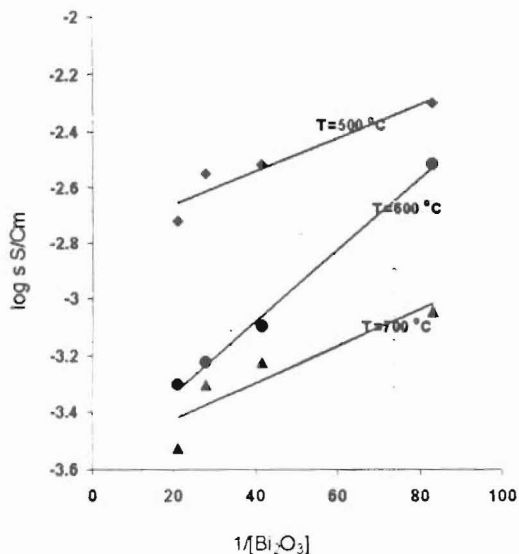


Fig. 9. The effect of bismuth oxide concentration on ionic conductivity for LSGM 9182 at different temperatures.

## 5. Conclusion

The glycine-nitrate combustion synthesis is a simple and convenient method to prepare LSGM 9182 powders. The thermal behaviour of LSGM 9182 pellets is brought out from the steady state sintering experiments to draw useful information on the inter-dependence of percentage shrinkage in volume and the percentage densification factor with respect to the maximum attainable apparent percentage porosity. The bulk conductivity value of LSGM 9182 is in the range of  $10^{-2}$  S/cm at temperature range between 500 and 800 °C Bismuth oxide found to be an effective sintering aid. Even though it has increased the densification, it decreases the conductivity value of LSGM 9182. According to Chakraborty [11], the added bismuth oxide was observed in LSGM pellets after heating at 1200 °C, 6 h. So we are going to focus on chemical and EPMA analyses to find out whether the bismuth oxide is going out or react with LSGM component.

## 6. Acknowledgement

The authors are very thankful to the Director, CECRI, Karaikudi for his interest in this work.

## 7. References

[1] T. Ishihara, H. Matsuda and Y. Takita, *J. Am. Chem. Soc.* **116**, 3801 (1994).

- [2] T. Ishihara, H. Matsuda and Y. Takita, *Solid State Ionics* **79**, 147 (1995).
- [3] T. Ishihara, Y. Hiei and Y. Takita, *Solid State Ionics* **79**, 371 (1995).
- [4] A. Petric, P. Huang and A. Skowron, in: *Proc. of the 2nd European Solid Oxide Fuel Cell Forum* (B. Thorestensen, Ed.) European SOFC Forum, Norway (1996) p. 751.
- [5] J. Drennan, V. Zelizko, D. Hay, F. Ciacchi, S. Rajendran and S. Badwal, *J. Mater. Chem.* **7**, 79 (1997).
- [6] J. Stevenson, T. Armstrong, D. McCready, L. Pederson, and W. Weber, *J. Electrochem. Soc.* **144**, 3613 (1997).
- [7] P. Huang, A. Petric, *J. Electrochem. Soc.* **143**, 1644 (1996).
- [8] J. Stevenson, T. Armstrong, L. Pederson, J. Li, C.A. Lewinsohn and S. Baskaran, *Solid State Ionics* **113-115**, 571 (1998).
- [9] M. Feng and J.B. Goodenough, *Euro. J. Solid State Inorg. Chem.* **T31**, 663 (1994).
- [10] K. Huang, R.S Tichy and J.B. Goodenough, *J. Am. Ceram. Soc.* **81**, 2576 (1998).
- [11] A. Chakraborty, and H.S. Maiti, *Ceramics International* **25**, 115 (1999).
- [12] A.K. Bhattachaya, A. Hartridge, K.K. Mallick and J.L. Woodhead, *Journal of Materials Science* **29**, 6076-6078 (1994).
- [13] *Chemistry of Solid State Materials: Chemical Synthesis of Advanced Ceramic Materials* by D. Segal, Cambridge University Press, Cambridge, p. 23.
- [14] K. Huang, M. Feng and J.B. Goodenough, *J. Electrochem. Soc.* **144**, 3620 (1997).
- [15] M. Feng and J.B. Goodenough, K. Huang and C. Milliken, *J. Power Sources* **63**, 47 (1996).
- [16] A. Ahmad-Khanlou, F. Tietz and D. Stöver, *Solid State Ionics* **135**, 543 (2000).
- [17] V.P. Gorelov, D.J. Bronin, Ju.V. Sokolova, H. Nafe and F. Aldinger, *J. Euro. Ceram. Soc.* **21**, 2311 (2001).

*Paper presented at the 2nd International Conference on Ionic Devices, Anna University, Chennai, India, Nov. 28-30, 2003.*

*Manuscript rec. Dec. 1, 2003; rev. Jan. 30, 2004; acc. Feb. 13, 2004.*